

## SEXTANS' COLD SUBSTRUCTURES AS A DYNAMICAL JUDGE: CORE, CUSP OR MOND?

V. LORA<sup>1</sup>, E. K. GREBEL<sup>1</sup>, F. J. SÁNCHEZ-SALCEDO<sup>2</sup> AND A. JUST<sup>1</sup>

*Draft version June 28, 2021*

### ABSTRACT

The cold dark matter model predicts cuspy dark matter halos. However, it has been found that, in some low-mass galaxies, cored dark halos provide a better description of their internal dynamics. Here we give constraints on the dark halo profile in the Sextans dwarf spheroidal galaxy by studying the longevity of two cold kinematic substructures detected in this galaxy. We perform  $N$ -body simulations of a stellar clump in the Sextans dwarf galaxy, including a live dark matter halo and the main stellar component. We find that, if the dark halo is cuspy, stellar clumps orbiting with semi-major axis  $\approx 400$  pc are disrupted in  $\sim 5$  Gyr, even if the clump is initially as compact stellar cluster with a radius of  $r_c = 5$  pc. Stellar clusters in an initial orbit with semi-major axis  $\leq 250$  pc may survive to dissolution but their orbits decay towards the center by dynamical friction. In contrast, the stellar clumps can persist for a Hubble time within a cored dark matter halo, even if the initial clump's radius is as extended as  $r_c = 80$  pc. We also study the evolution of the clump in the MONDian context. In this scenario, we find that even an extended stellar clump with radius  $r_c = 80$  pc survives for a Hubble time, but an unrealistic value for the stellar mass-to-light ratio of 9.2 is needed.

*Subject headings:* cosmology: dark matter – galaxies: dwarf – halos – kinematics and dynamics – methods: numerical

### 1. INTRODUCTION

The  $\Lambda$  cold dark matter ( $\Lambda$ CDM) model has proved to be successful in reproducing structure formation at large scales, but it faces some difficulties at galactic scales. For example, cosmological  $N$ -body simulations predict halos with a central cusp (Navarro et al. 1997; Moore et al. 1999; Jing & Suto 2000), whereas observations of the rotation curves of dwarf and low surface brightness galaxies indicate that a cored dark halo is preferred (van den Bosch et al. 2000; de Blok & Bosma 2002; Kuzio de Naray et al. 2008; de Blok et al. 2008; Donato et al. 2009).

Dwarf spheroidal (dSph) galaxies are the natural targets to study the properties of dark matter (DM) halos at very small masses. The analysis of the cusp-core controversy in dSph galaxies has motivated much work (Kleyna et al. 2003; Goerdt et al. 2006; Sánchez-Salcedo et al. 2006; Gilmore et al. 2007; Battaglia et al. 2008; Walker & Penarrubia 2011; Jardel & Gebhardt 2012; Salucci et al. 2012; Agnello & Evans 2012; Amorisco et al. 2013; Breddels & Helmi 2013). Dynamically cold stellar substructures as those observed in some dSph galaxies are sensitive probes of the gravitational potential. Kleyna et al. (2003) presented evidence that the stellar substructure in the Ursa Minor (UMi) dwarf spheroidal is incompatible with a cusped DM halo. They argued that the second peak located on the north-eastern side of the major axis of UMi is a disrupted stellar cluster that has survived in phase-space because the underlying gravitational potential is close to harmonic (Kleyna et al.

2003; Read et al. 2006; Sánchez-Salcedo & Lora 2007). This implies that the dark halo in UMi should have a cored mass density profile, instead of a cuspy mass profile as that predicted by the  $\Lambda$ CDM model, and that this core should be large (Kleyna et al. 2003; Lora et al. 2009). Lora et al. (2012) showed that the clump in UMi would be short lived if the dark halo were strongly substructured, but that it can survive for a Hubble time in a smooth halo with a large core.

There is also evidence of the existence of stellar kinematically cold substructures in the Sextans dSph galaxy. Kleyna et al. (2004) found a drop in the stellar velocity dispersion at their innermost data bin, which was interpreted as a dissolving cluster at the Sextans center. Later on, Walker et al. (2006) detected a region near Sextans core radius that appeared kinematically colder than the overall stellar population of Sextans, but they did not detect any signs of a kinematically distinct population at the center of Sextans. Recently, Battaglia et al. (2011) reported the detection of a cold substructure of very metal-poor stars close to the Sextans center. It remains unclear if this substructure is the same as that previously found in Kleyna et al. (2004).

Our main aim is to see if the longevity of the cold substructure found in Sextans can shed light onto the cusp-core controversy. In this work, we perform  $N$ -body simulations of the Sextans dSph galaxy. We model its stellar components (the main stellar component + stellar clump) and the DM halo. We explore different profiles for the DM halo and different sizes for the starting stellar clump. We also study the survivability of stellar substructures in Modified Newtonian Dynamics (MOND).

This article is organized as follows. In Section 2 we describe some properties of Sextans and their stellar clumps. The initial conditions for the  $N$ -body simulations are given in Section 3. The evolution of the substructures is described in Section 4. Finally, we discuss

vlor@ari.uni-heidelberg.de

<sup>1</sup>Astronomisches Rechen-Institut, Zentrum für Astronomie der Universität Heidelberg, Mönchhofstr. 12-14, 69120 Heidelberg, Germany

<sup>2</sup>Instituto de Astronomía, Universidad Nacional Autónoma de México, AP 70-264, 04510 D.F., México

the implications and give our conclusions in Section 5.

## 2. SEXTANS AND ITS KINEMATIC SUBSTRUCTURES

Sextans is a dSph galaxy satellite of the Milky Way. It is located at a Galactocentric distance of  $R_{GC} = 86$  kpc (Mateo 1998) and it has a luminosity of  $L_V = (4.37 \pm 1.69) \times 10^5 L_\odot$  (Lokas 2009). It has a core radius of  $R_{\text{core}} = 16.6$  arcmin ( $\sim 0.4$  kpc) and a tidal radius  $R_{\text{tidal}} = 160$  arcmin ( $\sim 4$  kpc) (Irwin & Hatzdimitriou 1995). Since the majority of the stars in Sextans are older than 10 Gyr (Lee et al. 2009), Karlsson et al. (2012) estimated the stellar mass of Sextans to be  $8.9 \pm 4.1 \times 10^5 M_\odot$  by integrating the light from a single 12 Gyr old stellar population. This mass is consistent with the value ( $8.5 \times 10^5 M_\odot$ ) obtained by Woo et al. (2008). The corresponding B-band stellar mass-to-light ratio is  $\Upsilon_* \approx 2$ .

The dynamical mass of Sextans has been estimated from the observed velocity dispersion profile. Assuming an isotropic velocity dispersion tensor and a Plummer model for the light distribution in Sextans, Kleyna et al. (2004) inferred that Sextans' total mass within 1 kpc lies between  $3 \times 10^7$  and  $1.5 \times 10^8 M_\odot$ . Adopting a NFW profile for the dark halo, Walker et al. (2007) obtained a dynamical mass of  $2.5 \times 10^7 M_\odot$  within a radius of 600 pc, whereas Strigari et al. (2007) estimated a total mass of  $0.9 \times 10^7 M_\odot$ , also within the central 600 pc. More recently, Lokas (2009) reported a total mass of  $(4.2 \pm 0.6) \times 10^7 M_\odot$  assuming an NFW density profile, which implies a  $M/L$  value of  $\sim 100$  (M/L) $_\odot$ . All these dynamical studies show that Sextans is a DM dominated dSph galaxy.

Here, we are interested in the existence of putative stellar substructures in Sextans. Kleyna et al. (2004) reported some evidence for a kinematically and photometrically distinct population at the Sextans center. These authors found that the dispersion at the center of Sextans was close to zero, and that such a change in the dispersion profile coincides with a change in the ratio of red horizontal branch stars to blue horizontal branch stars, i.e. in the stellar populations. They suggested that this is caused by the sinking and gradual dissolution of a stellar cluster at the center of Sextans.

In a later work, Walker et al. (2006) presented radial velocities of 294 possible Sextans members. Their larger data set did not confirm Kleyna et al.'s (2004) report of a kinematically distinct stellar population at the center of Sextans but they did obtain similar evidence when they restricted their analysis to a similar (small) number of stars as used by Kleyna et al. (2004). When considering their full radial velocity sample instead, Walker et al. (2006) detected a region near Sextans' core radius that is kinematically colder than the overall Sextans sample, with 95% confidence. They estimated a substructure luminosity of  $3 \times 10^4 L_\odot$ . We will refer to it as *substructure A*.

Recently, Battaglia et al. (2011) reported nine old stars that share very similar spatial location, kinematics and metallicities. The average metallicity of their 9-star group is low ( $[\text{Fe}/\text{H}] = -2.6$  dex with a 0.15 dex scatter), consistent with being the remnant of a old stellar cluster. This group of stars was taken from the six innermost metal-poor stars, which show a cold velocity dispersion of  $1.2 \text{ km s}^{-1}$  and an average velocity of  $72.5 \pm 1.3 \text{ km s}^{-1}$ .

Battaglia et al. (2011) suggested that the number of stars in this substructure (nine stars) is significant with respect to the total number of Sextans members for which spectroscopic measurements exist (174 stars). This substructure would account for 5% of Sextans' stellar population, which corresponds to a luminosity of  $2.2 \times 10^4 L_\odot$ . We will refer to it as *substructure B*.

The present spatial extent of the substructures is very uncertain. The contours of statistical significance for regions of cold kinematics in Walker et al. (2006) show that substructure A is centered on a location 15 arcmin north of the Sextans center and has a radial size of 4 arcmin ( $\sim 100$  pc). On the other hand, the nine innermost metal-poor stars that constitute the substructure B are found at  $R < 0^\circ.22$  (Battaglia et al. 2011), i.e. at  $\approx 330$  pc from the center of Sextans if we assume a distance to Sextans of 86 kpc. In Battaglia et al.'s (2011) data, there are no metal-poor stars at  $R < 0^\circ.1$ . This suggests that the substructure B extends in projected galactocentric radius from  $0^\circ.1$  to  $0^\circ.22$  (i.e. between 150 and 330 pc), indicating that, in projection, its center is at  $\sim 240$  pc from the Sextans center, and its radius is  $\sim 90$  pc at most.

## 3. THE N-BODY MODEL

### 3.1. Sextans' DM component

For our simulations, we constructed a live DM halo with a mass density profile given by

$$\rho(r) = \frac{\rho_0}{(r/r_s)^\gamma [1 + (r/r_s)^\alpha]^{(\beta-\gamma/\alpha)}}, \quad (1)$$

where  $r_s$  is the scale radius and  $\alpha$ ,  $\beta$  and  $\gamma$  define the DM halo's slope. This general density profile equation is very useful to define different density profiles. For example, a pseudo-isothermal sphere is obtained for  $(\alpha, \beta, \gamma) = (2, 0, 0)$  and an NFW profile is obtained for  $(\alpha, \beta, \gamma) = (1, 3, 1)$ .

We explored two different DM radial profiles: a pseudo-isothermal dark halo and an NFW halo. We adopted the parameters of Battaglia et al. (2011) for their best-fitting DM mass modeling of Sextans, based on their observed line-of-sight velocity dispersion profile. For a pseudo-isothermal DM halo, these authors found a core radius  $r_s = 3$  kpc, and a mass of  $4 \times 10^8 M_\odot$  within the last measured point ( $\sim 2.3$  kpc, assuming a distance to Sextans of 86 kpc). In this model, the DM mass within a radius of 0.6 kpc is  $0.9 \times 10^7 M_\odot$ . For the NFW DM halo, they derived a concentration  $c = 10$  and a virial mass  $M_V = 2.6 \times 10^9 M_\odot$ , resulting a DM mass within 0.6 kpc of  $2.6 \times 10^7 M_\odot$ .

To generate the initial conditions of the DM particles, we used the distribution function proposed by Widrow (2000), assuming an isotropic velocity dispersion tensor.

### 3.2. Sextans' main stellar component

The main stellar component in Sextans was modeled using the density profile

$$\rho_*(r) = \frac{(3-\gamma)M_*}{4\pi} \frac{a}{r^\gamma(r+a)^{\beta-\gamma}}, \quad (2)$$

where  $M_*$  is the total stellar mass and  $a$  is the scale radius. We set  $M_* \approx 9 \times 10^5 M_\odot$ , assuming a typical

value of the mass-to-light ratio  $\Upsilon_* = 2$ . We took  $\beta = 4$ , which corresponds to the Dehnen models (Dehnen 1993; Tremaine et al. 1994). In these models, the density declines as  $r^{-4}$  at large radii and diverges in the center as  $r^{-\gamma}$ . We used  $\gamma = 3/2$ , because it most closely resembles the de Vaucouleurs model in surface density. We took the scale radius for the main stellar component in the Sextans galaxy to be  $a \approx 0.4$  kpc (16.6 arcmin, Irwin & Hatzidimitriou 1995; Lokas 2009).

Battaglia et al. (2011) conducted an anisotropy study of Sextans and found that the general trend for the best-fitting DM mass model is to have a constant anisotropy value close to zero. Thus, the velocity dispersion of the main stellar component was taken to be isotropic.

We performed an  $N$ -body simulation with the DM halo (cored and NFW) and the main stellar component together. Each component was found to be stationary for a Hubble time (i.e., the density profile of the stellar component and its velocity dispersion stayed approximately constant for a Hubble time).

### 3.3. Sextans' stellar clumps

Our starting hypothesis is that the cold substructures in Sextans were initially stellar clusters that are now in the process of *very slow* dissolution. The substructures are the gravitationally unbound remnants of the stellar clusters. Adopting  $\Upsilon_* = 2$ , typical for an old stellar population, the mass in the substructures lies between  $M = 4.4 \times 10^4 M_\odot$  for substructure B to  $\simeq 6 \times 10^4 M_\odot$  for substructure A, which are reasonable for stellar clusters. In all our runs, we assumed, for simplicity, a fixed mass of  $4.4 \times 10^4 M_\odot$  for the initial stellar cluster.

For the initial density profile of the stellar clumps, we used a Plummer model, where the mass density profile is given by the following equation:

$$\rho_c(r) = \rho_0 \left( 1 + \frac{r^2}{r_c^2} \right)^{-5/2}, \quad (3)$$

(Plummer 1911). We explored different values for the initial core radius  $r_c$  between 5 pc, which corresponds to the size of a typical stellar cluster, and 80 pc, which is of the order of the present size of the observed substructures. Simulations with initial core radius of  $r_c = 5$  pc are aimed to represent a scenario where the stellar cluster has been caught in the last stage of tidal disruption. This scenario may present a timing problem because this stage is expected to proceed on a time-scale of one crossing time of the system and, thus, it would be very unlikely to observe them during this phase. Simulations with an initial radius of  $r_c = 80$  pc correspond to a situation where the stellar cluster became unbound immediately after formation due to supernova ejection of gas (Goodwin 1997).

Without the loss of generality, we set the clumps with an orbit in the  $(x, y)$  plane. Since we do not know the orbital parameters of the substructures, we explored different orbits for the clumps around the Sextans center. We only know lower limits for the semimajor axes of the substructures (it is  $\gtrsim 400$  pc for substructure A and  $\gtrsim 200$  pc for substructure B). Because projection effects lead to an underestimation of the galactocentric distance of the objects, there is a probability of 20% that the substructure B is at a deprojected distance of  $\geq 400$  pc to

Sextans' center. Therefore, since either substructure A or B or both may be on an orbit with a characteristic radius of 400 pc, we considered orbits with this size. Note that a distance of  $\sim 400$  pc corresponds to the core radius of the main stellar component in Sextans (see Section 2). We also considered the limiting case where the galactocentric distance of the clump is 250 pc in order to study a wider range of possible orbits of the clump; this case is relevant for substructure B. Since the substructures are not necessarily on circular orbits; it is also worthwhile to consider eccentric orbits.

### 3.4. The code

Since the internal two-body relaxation timescales for the three components (clump, main stellar component and halo) are much larger than a Hubble time, Sextans can be represented as collisionless (Binney & Tremaine 2008). We simulated the evolution of the Sextans dwarf galaxy (stellar clump, main stellar component and DM halo) using the  $N$ -body code SUPERBOX (Fellhauer et al. 2000; Bien et al. 2013). SUPERBOX is a highly efficient particle-mesh, collisionless-dynamics code with high resolution sub-grids.

In our case, SUPERBOX uses three nested grids centered on the center of density of the Sextans dSph galaxy. We used  $128^3$  cubic cells for each of the grids. The inner grid is meant to resolve the inner region of Sextans and the outer grid (with radii of 100 kpc for all cases) resolves the stars that are stripped away from Sextans' potential. The tidal field created by the Milky Way was not included. The spatial resolution is determined by the number of grid cells per dimension ( $N_c$ ) and the grid radius ( $r_{\text{grid}}$ ). Then the side length of one grid cell is defined as  $l = \frac{2r_{\text{grid}}}{N_c - 4}$ . For  $N_c = 128$ , the resolution is of the order of the typical distance between the particles in the simulation.

SUPERBOX integrates the equations of motion with a leap-frog algorithm, and a constant time step  $dt$ . We selected a time step of  $dt = 0.1$  Myr in our simulations in order to guarantee that the energy (for the isolated components) is conserved better than 1%.

## 4. RESULTS

Our  $N$ -body simulations were carried out from an integration time  $t = 0$  to  $t = 10$  Gyr. We used  $1 \times 10^7$  particles to model each of the DM halos,  $1 \times 10^5$  particles to model the main stellar component, and  $1 \times 10^4$  particles to model the stellar clump. The parameters of our 14 models, from  $M1$  to  $M14$ , are summarized in Table 1.

### 4.1. The cored DM halo case

We first consider the evolution of the clump when it is embedded in a pseudo-isothermal DM halo, having a core radius  $r_s = 3$  kpc and a mass within 0.6 kpc of  $0.9 \times 10^7 M_\odot$  (see Section 3.1). In order to visualize the evolution of the clump in Sextans, we built a map of the surface density (in units of  $M_\odot \text{pc}^{-2}$ ) of the stellar clump in the  $(x, y)$ -plane. Figure 1 shows the temporal evolution of the mass surface density of the clump in the models  $M1$  (clump radius  $r_c = 12$  pc) and  $M2$  (clump radius  $r_c = 80$  pc) for the cored DM halo. The white circle shows the initial orbit of the stellar clump, and the white cross shows the center of Sextans.

Model *M1* represents a case where the initial clump is very compact; it resembles the globular clusters found in the Fornax dSph galaxy (Mackey & Gilmore 2003; Peñarrubia et al. 2009), which have core radii ranging from 1.4 to 10 pc. In *M1*, the stellar cluster remains essentially intact over the duration of the run, 10 Gyr (see Figure 1), because the tidal heating by the parent galaxy’s halo is very low.

Unbound clumps as extended as the observed substructures (our model *M2*) also remain essentially unaltered for 10 Gyr (see the bottom panels of Figure 1). The physical reason is that the underlying potential within the DM core is harmonic and, therefore, the substructure is long-lived even if it is a gravitationally unbound system (Kleyna et al. 2003; Lora et al. 2009). We also checked that the substructure can persist for a long time if it is dropped on a circular orbit with a radius of 250 pc (simulation *M3*). Therefore, we concluded that a dark halo with core radii of  $\gtrsim 3$  kpc may host unbound cold substructures as those observed in Sextans.

#### 4.2. The NFW DM halo case

The top panels of Figure 2 show the evolution of the mass surface density of the stellar clump with initial radius  $r_c = 12$  pc (model *M4*), in a NFW halo with a concentration  $c = 10$  and a virial mass of  $M_V = 2.6 \times 10^9 M_\odot$  (see Section 3.1). For the first 3 Gyr, the stellar clump appears almost unperturbed (see panel (c) of Figure 2), but after 5 Gyr the orbital phase mixing dissolves it completely and so only a tidal debris can be seen in panel (d) of Figure 2.

The lower panels of Figure 2 show four snapshots of the substructure when its initial radius is  $r_c = 80$  pc (model *M5*). The clump is disrupted in  $\sim 0.5$  Gyr because of the tidal forces by the parent DM halo. Since this time is much shorter than its age ( $\sim 10$  Gyr), the substructure is short lived.

At any given time  $t$  in the simulation we sample the two-dimensional map searching for the  $10 \times 10$  pc size parcel that contains the highest mass (number of clump particles). We define the destruction time as the time at which the parcel with the highest mass surface density has reached a value of  $\sim 1 M_\odot \text{pc}^{-2}$ . When such value is reached, the column density of the clump is so low that it would be indistinguishable from Sextans’ main stellar component, and would thus be undetectable. In Figure 3, we plot the surface density of this parcel as a function of time. We see that the destruction time is  $\sim 4.4$  Gyr in model *M4* and  $\sim 0.45$  Gyr in model *M5*.

In model *M6*, we reduced the initial size of the clump to a radius  $r_c = 5$  pc (Figure 4). We found that not even with such a small clump is able to survive for more than  $\sim 5$  Gyr.

In order to study the effect of the orbital eccentricity on the destruction time, we ran two simulations (*M7-M8*, see Table 1) where clump’s orbit is non-circular. In model *M7*, we set the 5 pc radius clump in a pure radial orbit with apocenter at 400 pc (see Figure 6). We found that the clump loses its identity in 4 Gyr (Figure 6). In model *M8*, we set the 5 pc radius cluster at a radial distance of 400 pc with a tangential velocity twice the circular velocity at that distance ( $v_y = 2 \times v_c$ ). Thus, the orbit is eccentric and its pericenter is located at 400 pc. In this case, the clump is disrupted within  $\sim 5$  Gyr.

Therefore, it is difficult to explain the existence of cold substructures in Sextans at projected distances of  $\sim 400$  pc, as substructure A, if an NFW profile is adopted for its DM halo.

In the case of substructure B, its projected distance is uncertain and we cannot rule out orbital radii of  $\sim 200$  pc or less. In order to explore if this clump could survive for a significant time, we ran a simulation (*M9*) where a 5 pc radius cluster is set on a circular orbit with a radius of 250 pc. In this case, the clump starts to lose particles while it spirals to the center of Sextans DM potential due to dynamical friction. At  $t \approx 3$  Gyr, the stellar clump reaches the center of Sextans, and it keeps orbiting very close to the center until the end of the simulation (see Figure 5). As a consequence, the stellar clump survives as a central star cluster. It has to be noticed that the dissolution of the clump in this case is similar to model *M6* only during the first  $\sim 3$  Gyr.

The evolution of the clump occurs in a similar manner in model *M10*, where the orbit of the 5 pc radius clump has its apocenter at 250 pc and its pericenter at 100 pc. The clump spirals to the center of Sextans and loses mass, until the density of the clump decreases by a factor of  $\sim 2$  at  $t \approx 1$  Gyr (see Figure 5). After this time, the orbital radius of the clump lies between 30 and 90 pc and its dissolution proceeds in a very slowly way.

We conclude that cold substructures having initial orbital radii of  $\sim 400$  pc would not survive in an NFW halo. Only substructures with initial orbital radii  $\lesssim 300$  pc could survive but they should be located close to the Sextans center (distances  $< 100$  pc) because of the orbital decay due to dynamical friction. Since substructure A is at a projected distance of 400 pc, it is difficult to understand how it survived against mixing in an NFW halo. A more accurate determination of the projected distance of substructure B would be very important to constrain the models further.

#### 4.3. The case of MOND

It is interesting to explore if the gravitational potential predicted in MOND could explain the survival of cold substructures. To do so, we followed a similar treatment as in Sánchez-Salcedo & Lora (2010) for the UMi dSph galaxy. In the MOND framework, the gravitational potential that describes the force acting on a star in Sextans follows the modified Poisson equation of Bekenstein & Milgrom (1984)

$$\nabla \cdot [\mu(x)\nabla\Phi] = 4\pi G\rho, \quad (4)$$

where  $x = |\nabla\Phi|/a_0$ ,  $a_0 \simeq 1.2 \times 10^{-8} \text{ cm s}^{-2}$  is the universal acceleration constant of the MOND theory, and  $\mu(x)$  is the interpolating function, which runs smoothly from  $\mu(x) = x$  at  $x \ll 1$  to  $\mu(x) = 1$  at  $x \gg 1$ . The differential equation (4) must be solved with the boundary condition  $\nabla\phi \rightarrow -\mathbf{g}_E$ , where  $\mathbf{g}_E$  is the external gravity acting on Sextans and has a magnitude  $g_E = V^2/R_{GC}$ .  $V$  is the Galactic rotational velocity at  $R_{GC}$  which coincides with the asymptotic rotation velocity  $V_\infty$  for the Milky Way. We set this value to  $V_\infty = 170 \text{ km s}^{-1}$  which is obtained by adopting a mass model for the Milky Way under MOND (Famaey & Binney 2005; Sánchez-Salcedo & Hernandez 2007).

A star in the stellar clump of Sextans feels the external acceleration created by the Milky Way (denoted by  $\mathbf{g}_E$ ), the acceleration generated by Sextans smooth stellar component ( $\mathbf{g}_I$ ), and the acceleration generated by all other stars that form the stellar clump ( $\mathbf{g}_{int}$ ), and thus all must be taken in consideration.

Since the circular velocity of a test particle at the stellar core radius ( $r_* \simeq 0.4$  kpc) of Sextans is  $\sim 5.9$  km s $^{-1}$ , then the characteristic internal acceleration  $[v_c(r_*)]^2/r_* \simeq 2.9 \times 10^{-10}$  cm s $^{-2}$ . This is much smaller than MOND's characteristic acceleration  $a_0 \simeq 1.2 \times 10^{-8}$  cm s $^{-2}$ . Moreover, the external acceleration,  $V_\infty^2/R_{GC} \simeq 0.11 \times 10^{-8}$  cm s $^{-2}$  is also much smaller than  $a_0$ . We can conclude then that the Sextans internal dynamics lies deep in the MOND regime. The ratio between the internal acceleration at Sextans' stellar core radius and the external acceleration ( $g_I/g_E \approx 0.26$ ) tells us that the dynamics in Sextans is dominated by the external field ( $g_E \gg g_I$ ).

Sánchez-Salcedo & Hernandez (2007) studied the dSph galaxies of the Milky Way under MOND and compared the results with DM halos. For Sextans, they obtained a high value of (M/L) of  $\sim 7.5 - 36$  assuming that the external field is dominant in this galaxy. Angus (2008) analyzed the line-of-sight velocity dispersion as a function of radius for eight Milky Way dSph galaxies and calculated the mass-to-light ratio in the MONDian regime through a Jeans analysis. He found that Sextans requires a rather high mass-to-light ratio of 9.2. We adopted this value here.

We carried out  $N$ -body simulations under the MOND approximation with the code described in Section 3 starting with clumps of different radii ( $r_c = 12, 35$  and  $80$  pc, which correspond to models  $M11, M12$  and  $M13$ , respectively). The parameters of the different models are summarized in Tables 1 and 2. The clump survives for more than 10 Gyr in the three cases (see Figure 3). It is interesting to note that when the initial stellar clump is extended ( $r_c = 80$  pc), it spirals to the center of Sextans; at  $t = 10$  Gyr it orbits within  $\sim 0.3$  kpc. This is clearly seen in Figure 7.

Finally, we ran a simulation ( $M14$ ) of the 80 pc radius clump in a circular orbit with a galactocentric distance of 250 pc. Also in this case the clump remains undisturbed for 10 Gyr. In this case, the clump also spirals to the center of Sextans, and at  $t = 10$  Gyr it orbits within  $\sim 0.2$  kpc.

## 5. CONCLUDING REMARKS

Using  $N$ -body simulations, we studied the survival of cold kinematic substructures in the DM halo of the Sextans dwarf galaxy against phase mixing. We compared the evolution of substructures when the dark halo has a core and when the dark halo follows the NFW profile,

those having the parameters derived by Battaglia et al. (2011) to explain the projected velocity dispersion profile. We found that the core in the pseudoisothermal model is large enough to make the potential almost harmonic and, thus, to guarantee the survival of substructures. Even if the clump is initially very extended ( $r_c = 80$  pc), it easily survives for 10 Gyr. We conclude that the stellar clump in Sextans is in agreement with a cored DM halo.

On the contrary, stellar clumps orbiting with semi-major axes of  $\sim 400$  pc and initial Plummer radii between 12 and 80 pc are destroyed if they are embedded in the NFW DM halo. Not even a stellar clump with a small Plummer radius of  $r_c = 5$  pc (model  $M6$ ) can survive in such a NFW DM halo. Stellar clumps initially orbiting at a radius  $\leq 250$  pc from the Sextans center spiral to the center due to dynamical friction and, as a consequence, phase mixing is reduced. Clumps in these orbits may survive but would merge forming a central star cluster at the center of Sextans.

It has to be noted that we cannot rule out a scenario where the DM profile was initially cuspy and evolved to a cored halo. For instance, energy feedback from supernova explosions and stellar winds, may lead severe gravitational potential fluctuations, which may reduce the central mass density of dwarf galaxies (e.g., Mashchenko et al. (2008)). Similarly, Pasetto et al. (2010) found that initial cuspy DM profiles flatten with time as a result of star formation, which would explain the observations without contradicting a cuspy DM profile. On the other hand, Peñarrubia et al. (2012) show some difficulties with the fine-tuning of the scenarios just mentioned. Goerdts et al. (2010) discuss that the transfer of energy from sinking massive objects may destroy central cusps.

As a last point, we investigated whether or not the clump in Sextans could survive in the MONDian framework. We found that even a stellar clump with  $r_c = 80$  pc remains undisturbed for a Hubble time and slowly spirals to the center of Sextans. However, it has to be noticed that the adopted MOND value for the stellar mass-to-light ratio of  $M/L_V = 9.2$ , which was derived by Angus (2008) to explain the observed velocity dispersion profile of Sextans, is very high and inconsistent with the properties expected from an old purely stellar population.

## ACKNOWLEDGMENTS

We wish to thank the anonymous referee for very useful comments that greatly improved the content of this paper. V.L. gratefully acknowledges support from an Alexander von Humboldt Foundation fellowship and the FRONTIER grant. F.J.S.S. acknowledges financial support from CONACyT project 165584 and PAPIIT project IN106212.

## REFERENCES

- Agnello, A., & Evans, N. W. 2012, ApJ, 754, L39  
 Amorisco, N. C., Agnello, A., & Evans, N. W. 2013, MNRAS, 429, L89  
 Angus, G. W. 2008, MNRAS, 387, 1481  
 Battaglia, G., Helmi, A., Tolstoy, E., Irwin, M., Hill, V., & Jablonka, P. 2008, ApJ, 681, L13  
 Battaglia, G., Tolstoy, E., Helmi, A., Irwin, M., Parisi, P., Hill, V. & Jablonka, P. 2011, MNRAS, 411, 1013  
 Bekenstein, J. & Milgrom, M. 1984, ApJ, 286, 7  
 Bien, R., Brandt, T. & Just, A. 2013, MNRAS, 428, 1631  
 Binney, J., & Tremaine, S. 2008, Galactic Dynamics, 2nd edn. Princeton Univ. Press, Princeton, New Jersey  
 Breddels, M. A., & Helmi, A. 2013, arXiv:1304.2976  
 de Blok, W. J. G., & Bosma, A. 2002, A&A, 385, 816  
 de Blok, W. J. G., Walter, F., Brinks, E., Trachternach, C., Oh, S.-H., & Kennicutt, R. C., Jr. 2008, AJ, 136, 2648  
 Mashchenko, S., Couchman, H. M. P., & Wadsley, J. 2006, Nature, 442, 539

- Dehnen, W. 1993, MNRAS, 265, 250
- Donato, F., Gentile, G., Salucci, P., Martins, C. F., Wilkinson, M. I., Gilmore, G., Grebel, E. K., Koch, A. & Wyse, R. 2009, MNRAS, 397, 1169
- Famaey, B., & Binney, J. 2005, MNRAS, 363, 603
- Fellhauer, M., Kroupa, P., Baumgardt, H., Bien, R., Boily, C. M., Spurzem, R. & Wassmer, N. 2000, New Astron., 5, 305
- Gilmore, G., Wilkinson, M., Kley, J., Koch, A., Evans, W., Wyse, R. F. G. & Grebel, E. K. 2007, NuPhS, 173, 15
- Goerdt, T., Moore, B., Read, J. I., Stadel, J. & Zemp, M. 2006, MNRAS, 368, 1073
- Goerdt, T., Moore, B., Read, J. I. & Stadel, J. 2010, ApJ, 725, 1707
- Goodwin, S. P. 1997, MNRAS, 286, 669
- Irwin, M. & Hatzidimitriou, D. 1995, MNRAS, 277, 1354
- Jardel, J. R., & Gebhardt, K. 2012, ApJ, 746, 89
- Jing, Y. P., & Suto, Y. 2000, ApJ, 529, L69
- Karlsson, T., Bland-Hawthorn, J., Freeman, K. & Silk, J. 2012, ApJ, 759, 111
- Kley, J. T., Wilkinson, M. I., Evans, N. W. & Gilmore G. 2004, MNRAS, 354, L66
- Kley, J. T., Wilkinson, M. I., Gilmore, G. & Evans, N. W. 2003, ApJ, 588L, 21
- Klypin, A., Kravtsov, A. V., Valenzuela, O. & Prada, F. 1999, ApJ, 522, 82
- Kuzio de Naray, R., McGaugh, S. S., de Blok, W. J. G. 2008, ApJ, 676, 920
- Lee, M. G., Yuk, I.-S., Park, H. S., Harris, J. & Zaritsky D. 2009, ApJ, 703, 692
- Lokas, E. L. 2009, MNRAS, 394, L102
- Lora, V., Sánchez-Salcedo, F. J., Raga, A. C. & Esquivel, A. 2009, ApJ, 699, L113
- Lora, V., Just, A., Sánchez-Salcedo, F. J. & Grebel, E. K. 2012, ApJ, 757, 87
- Mackey, A. D. & Gilmore, G. F. 2003, MNRAS, 340, 175
- Mateo, M. L. 1998, ARA&A, 36, 435
- Moore, B., Quinn, T., Governato, F., Stadel, J., & Lake, G. 1999, MNRAS, 310, 1147
- Navarro, J. F., Frenk, C. S. & White, S. D. M. 1996, ApJ, 462, 563
- Navarro, J. F., Frenk, C. S. & White, S. D. M. 1997, ApJ, 490, 493
- Pasetto, S., Grebel, E. K., Berczik, P., Spurzem, R. & Dehnen, W. 2010, A&A, 514, 47
- Peñarrubia, J., Walker, M. G. & Gilmore, G. 2009, MNRAS, 399, 1275
- Peñarrubia, J., Koposov, S. E. & Walker, M. G. 2012, ApJ, 760, 2
- Plummer, H. C. 1911, MNRAS, 71, 460
- Read, J. I., Wilkinson, M. I., Evans, N. W., Gilmore, G. & Kley, J. T. 2006, MNRAS, 367, 387
- Salucci, P., Wilkinson, M. I., Walker, M. G., Gilmore, G. F., Grebel, E. K., Koch, A., Martins, C. F. & Wyse, F. G. 2012, MNRAS, 420, 2034
- Sánchez-Salcedo, F. J., Reyes-Iturbide, J. & Hernandez, X. 2006, MNRAS, 370, 1829
- Sánchez-Salcedo, F. J. & Hernandez, X. 2007, ApJ, 667, 878
- Sánchez-Salcedo, F. J. & Lora, V. 2007, ApJ, 658, L83
- Sánchez-Salcedo, F. J. & Lora, V. 2010, MNRAS, 407, 1135
- Strigari, L. E., Bullock, J. S., Kaplinghat, M., Diemand, J., Kuhlen, K. & Madau, P. 2007, ApJ, 669, 676
- Tremaine, S., Richstone, D. O., Byun, Y.I., et al. 1994, AJ, 107, 634
- van den Bosch, F. C., Robertson, B. E., Dalcanton, J. J. & de Blok, W. J. G. 2000, AJ, 119, 1579
- Walker, M. G., Mateo, M., Olszewski, E. W., Pal, J. K., Sen, B. & Woodroffe, M. 2006, ApJ 642, L41
- Walker, M. G., Mateo, M., Olszewski, E. W., Gnedin, O. Y., Wang, X., sen, B. & Woodroffe, M. 2007, ApJ 667, L53
- Walker, M. G., & Penarrubia, J. 2011, ApJ, 742, 20
- Woo, J., Courteau, S. & Dekel, A. 2008, MNRAS 390, 1453
- Widrow, L. M. 2000, ApJS, 131, 39

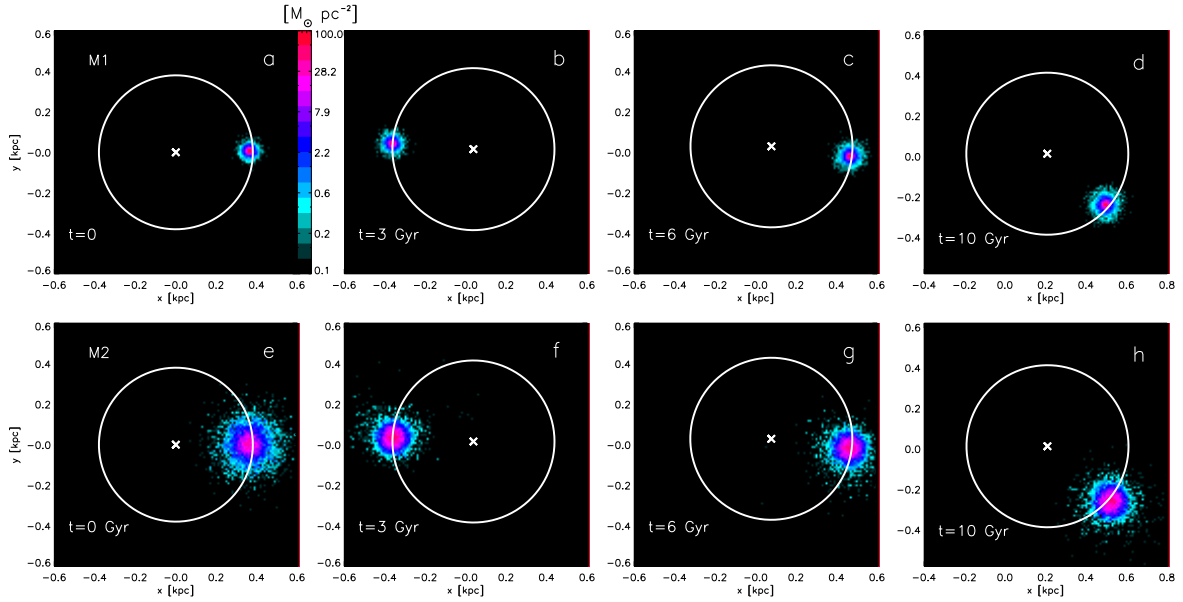


FIG. 1.— Time evolution ( $t = 0, 3, 6$  and  $10$  Gyr) of the stellar clump’s mass surface density in the Sextans dSph galaxy. The top panels show the evolution of the clump in model *M1* ( $r_c = 80$  pc), whereas the bottom panels show the evolution of the clump in model *M2* ( $r_c = 80$  pc). The white circle shows the initial orbit with  $0.4$  kpc radius. The white cross marks the center of Sextans. The main stellar component is not shown.

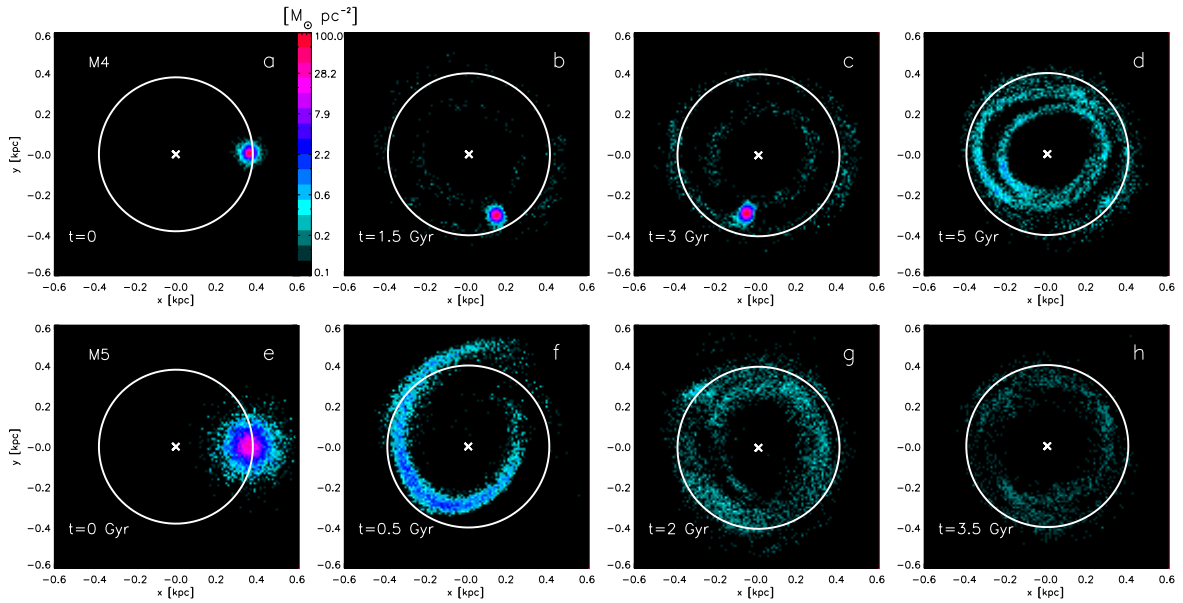


FIG. 2.— The top panels show the mass surface density of Sextans’ stellar clump at four different times ( $t = 0, 1.5, 3$  and  $5$  Gyr) in model *M4* ( $r_c = 12$  pc). In the bottom panels, we show the mass surface density (at  $t = 0, 0.5, 2$  and  $3.5$  Gyr) of model *M5* ( $r_c = 80$  pc). The white circle shows the initial orbit. The white cross marks the center of Sextans.

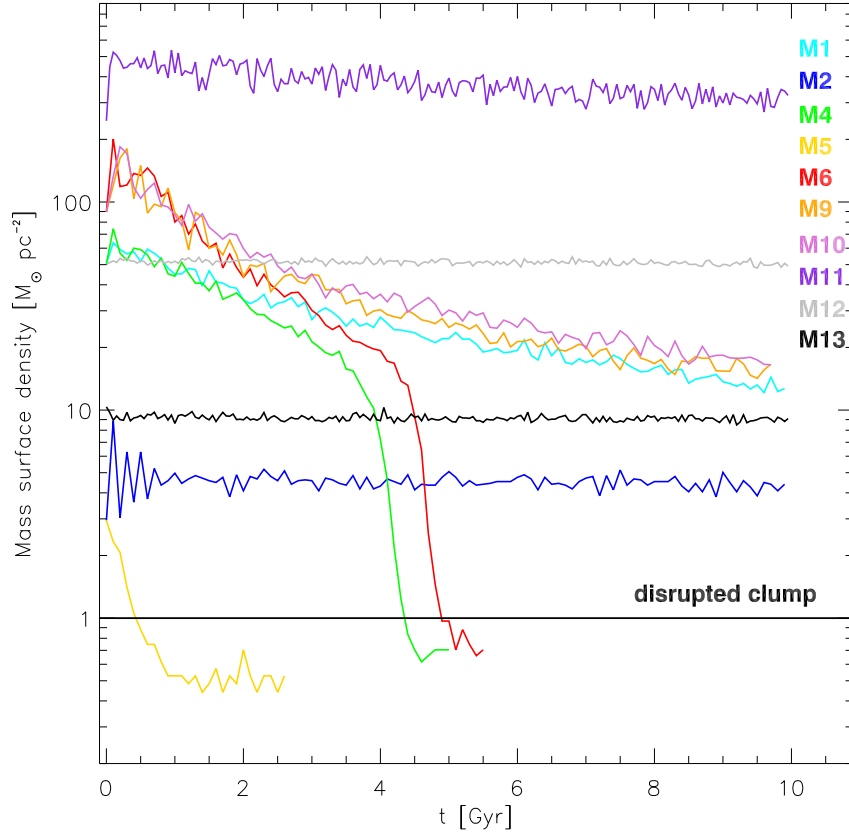


FIG. 3.— Mass surface density of Sextans’ stellar clump mapped in the  $(x, y)$ -plane as a function of time, for the models quoted at the right margin of the Figure (see Table 1).

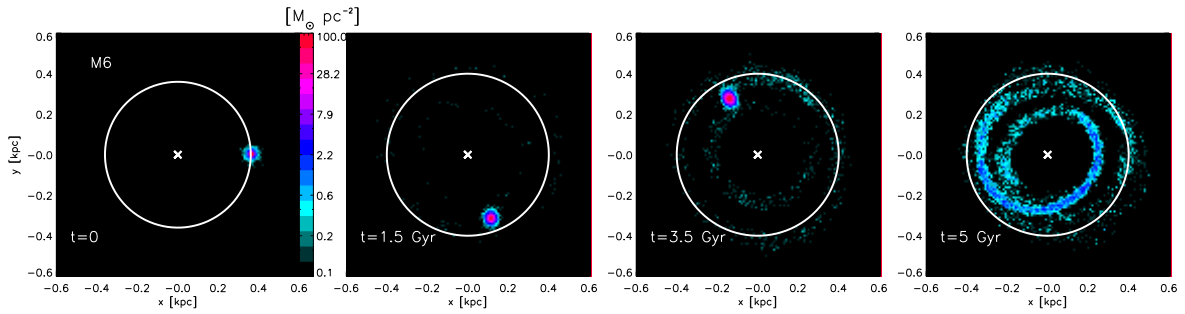


FIG. 4.— Mass surface density of Sextans stellar clump in the  $(x, y)$ -plane in model  $M6$  for the integration times  $t = 0, 1.5, 3.5$  and  $5$  Gyr. The white circle shows the initial orbit with  $0.4$  kpc radius. The white cross marks the center of Sextans.



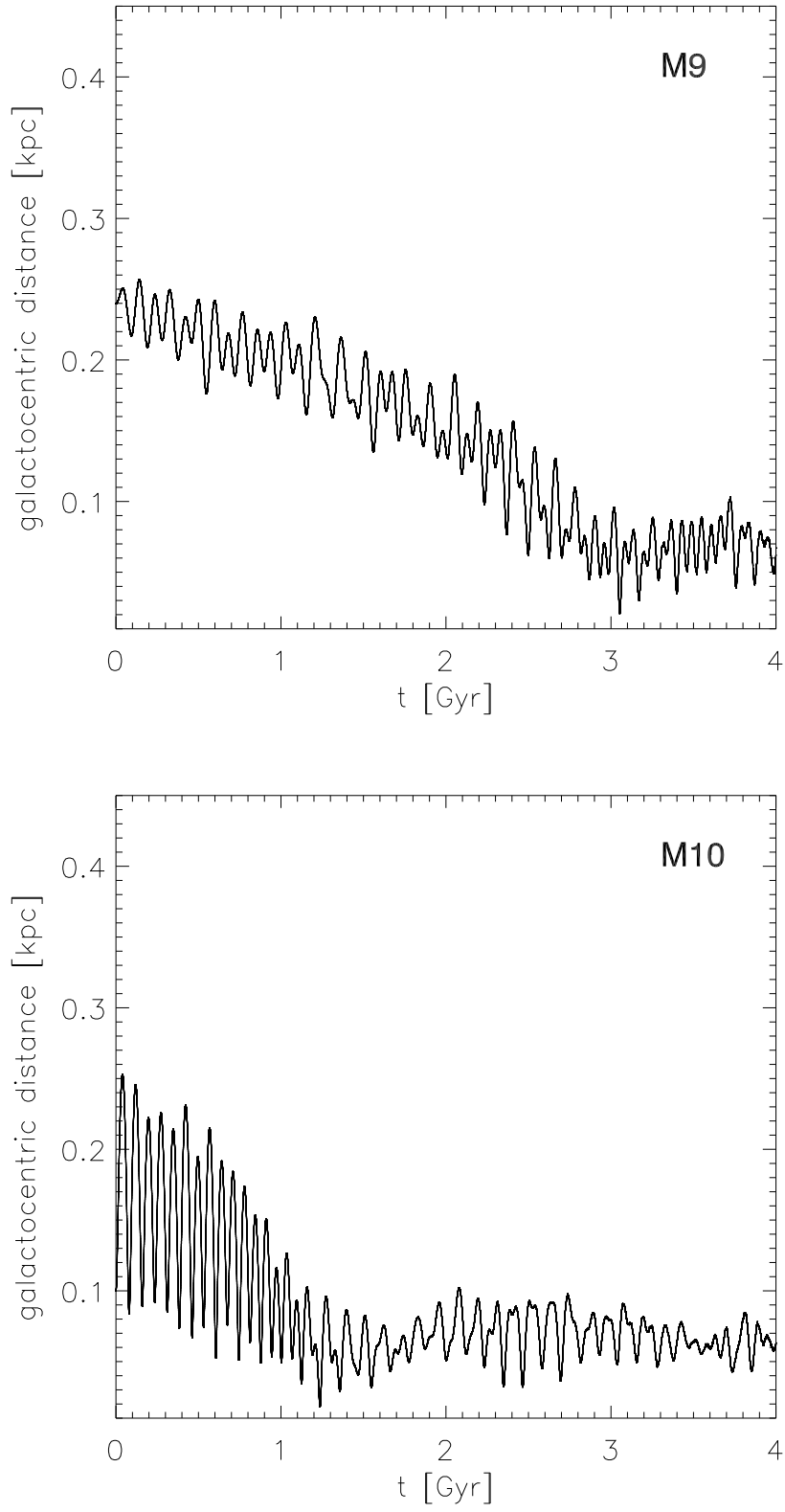


FIG. 5.— Galactocentric distance of the clump as a function of time, for models *M9* (top panel) and *M10* (bottom panel).

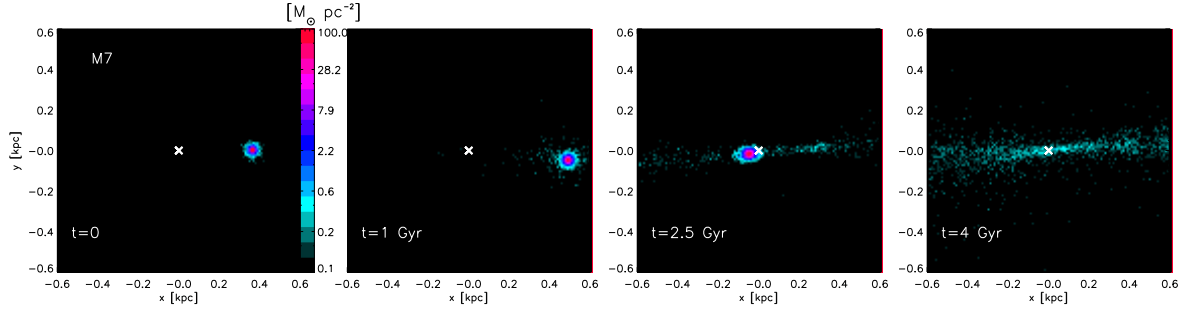


FIG. 6.— Mass surface density of Sextans stellar clump in the plane of the orbit, in model *M7* for the integration times  $t = 0, 1, 2.5$  and  $4$  Gyr. The white cross marks the center of Sextans.

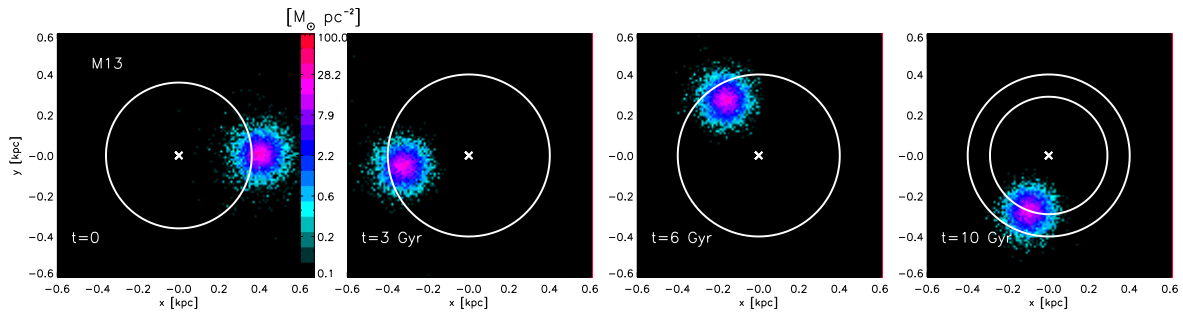


FIG. 7.— Mass surface density of Sextans stellar clump in the  $(x, y)$ -plane in model *M13* for the integration times  $t = 0, 3, 6$  and  $10$  Gyr. The outer white circle shows the initial orbit of the stellar clump, with  $0.4$  kpc radius. The inner circle shows the final orbit with a radius of  $0.29$  kpc.

TABLE 1  
PARAMETERS OF THE MODELS

Model	Halo profile <sup>a</sup>	$r_c$ [pc]	Surviving time [Gyr]	Type of orbit
M1	ISO	12	$> 10$	circular orbit of radius of 400 pc
M2	ISO	80	$> 10$	circular orbit of radius of 400 pc
M3	ISO	80	$> 10$	circular orbit of radius of 250 pc
M4	NFW	12	$\sim 4.4$	circular orbit of radius of 400 pc
M5	NFW	80	$\sim 0.45$	circular orbit of radius of 400 pc
M6	NFW	5	$\sim 5$	circular orbit of radius of 400 pc
M7	NFW	5	$\sim 4$	radial, apocenter at 400 pc
M8	NFW	5	$\sim 5$	eccentric, pericenter at 400 pc, velocity at pericenter: $v_x = 0, v_y = 2v_c$
M9	NFW	5	$> 10^b$	circular orbit of radius of 250 pc
M10	NFW	5	$> 10^c$	eccentric, apocenter at 250 pc and pericenter at 100 pc
M11	MOND	12	$> 10$	circular orbit of radius of 400 pc
M12	MOND	35	$> 10$	circular orbit of radius of 400 pc
M13	MOND	80	$> 10$	circular orbit of radius of 400 pc
M14	MOND	80	$> 10$	circular orbit of radius of 250 pc

<sup>a</sup>ISO refers to the pseudo-isothermal profile.

<sup>b</sup>The orbit decays to the Sextans center in  $\sim 3$  Gyr.

<sup>c</sup>The orbit decays to the Sextans center in  $\sim 1$  Gyr.

TABLE 2  
PARAMETERS OF THE SEXTANS dSPH AND ITS STELLAR CLUMP

Sextans	D [kpc]	$L_V$ [ $L_\odot$ ]	$r_*$ [arcmin]	$M_*$ [ $M_\odot$ ]	$M(< r_*)$ [ $M_\odot$ ]	$v_c(r_*)$ [km s $^{-1}$ ]	$g_I/g_E$ at $r_*$
	86	$4.37 \times 10^5$	16.6	$8.7 \times 10^5$	$3.18 \times 10^5$	5.9	0.26
Clump	Semi-major axis [kpc]	$L_V$ [ $L_\odot$ ]	$r_h$ [pc]	$M$ [ $M_\odot$ ]		$v_c(r_h)$ [km s $^{-1}$ ]	$g_{int}/g_E$ at $r_h$
Small clump	0.4	$2.2 \times 10^4$	15.6	$2.02 \times 10^5$		1.3	0.35
Big clump	0.4	$2.2 \times 10^4$	45.5	$2.02 \times 10^5$		1.8	0.10